Published in final edited form as:

J Am Chem Soc. 2024 April 03; 146(13): 8865–8876. doi:10.1021/jacs.3c09735.

A Transfer Hydrogenation Approach to Activity-Based Sensing of Formate in Living Cells

Steven W.M. Crossley[†,a], **Logan Tenney**[†,a], **Vanha N. Pham**[a], **Xiao Xie**[a], **Michelle W. Zhao**[a], **Christopher J. Chang**[*,a,b,c]

[a]Department of Chemistry, University of California, Berkeley, Berkeley, California, 94720, United States

[b]Department of Molecular and Cell Biology, University of California, Berkeley, Berkeley, California, 94720, United States

[c]Helen Wills Neuroscience Institute, University of California, Berkeley, Berkeley, California, 94720, United States

Abstract

Formate is a major reactive carbon species in one-carbon metabolism, where it serves as an endogenous precursor for amino acid and nucleic acid biosynthesis and a cellular source of NAD(P)H. On the other hand, aberrant elevations in cellular formate are connected to progression of serious diseases, including cancer and Alzheimer's disease. Traditional methods for formate detection in biological environments often rely on sample destruction and/or extensive processing, resulting in a loss of spatiotemporal information. To help address these limitations, here we present the design, synthesis, and biological evaluation of a first-generation activity-based sensing system for live-cell formate imaging that relies on iridium-mediated transfer hydrogenation chemistry. Formate facilitates an aldehyde-to-alcohol conversion on various fluorophore scaffolds to enable fluorescence detection of this one-carbon unit, including through a two-color ratiometric response with internal calibration. The resulting two-component probe system can detect changes in formate levels in living cells with high selectivity over potentially competing biological analytes. Moreover, this activity-based sensing system can visualize changes in endogenous formate fluxes through alterations of one-carbon pathways in cell-based models of human colon cancer, presaging the potential utility of this chemical approach to probe the continuum between one-carbon metabolism and signaling in cancer and other diseases.

Graphical Abstract

[*]Corresponding Author: **Christopher J. Chang** – Department of Chemistry, Department of Molecular and Cell Biology, and Helen Wills Neuroscience Institute, University of California, Berkeley, Berkeley, California 94720, United States; chrischang@berkeley.edu.

Author Contributions

The manuscript was written through contributions of all authors. / All authors have given approval to the final version of the manuscript. / †These authors contributed equally.

[†]S.W.M.C. and L.T. contributed equally to this paper.

Supporting Information

The Supporting Information is available free of charge on the ACS Publications website. Synthetic, spectroscopic, and biological methods and data are provided (PDF).

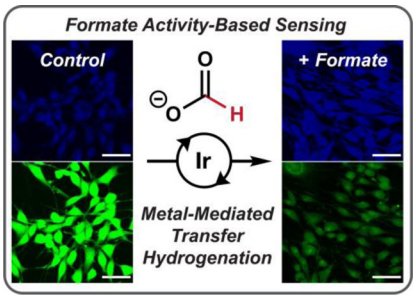

INTRODUCTION

One-carbon metabolism plays a central role in regulating cellular metabolism and epigenetics, but aberrations in one-carbon cycles are associated with the progression of serious diseases, including diabetes, chronic liver and heart diseases, neurodegenerative diseases, and cancer.[1,2,3,4,5] In this context, formate is a primary one-carbon unit that is produced, utilized, and regulated within one-carbon metabolic cycles and is essential for sustaining amino acid (serine, glycine, methionine) and nucleotide (purine/thymidylate) biosynthesis, as well as redox, energy, and epigenetic homeostasis.[1,2,3,4,5] In mammals, formate concentrations normally reside in range of 10–100 μM in blood[1] and can rise to above 1 mM within cells;[6] moreover, its levels can fluctuate greatly between healthy and diseased states.[4,5] Indeed, increased formate overflow is a potential biomarker for neurodegenerative Alzheimer's disease[7] and a hallmark of oxidative stress in cancer.[8] In one striking clinical study, formate was posited as a potential biomarker for esophageal cancer progression, with the observation that formate levels progressively increased in esophageal tumors relative to normal mucosae from Stage I (8.45x) to Stage II (13.51x) to Stage III (14.84x) to Stage IV (21.48x).[9]

Despite its significant contributions to the fundamental chemistry of the cell and potential translational applications to medicine, methods for monitoring formate within intact, living biological specimens remain underdeveloped. Along these lines, current methods for formate analysis in biological samples include its derivatization through amide bond formation to formyl-2-nitrophenyl-hydrazide for detection by LC-MS,[10,11] enzyme-mediated colorimetric detection in post-lysis specimens,[5,12] and NMR analysis,[9] all of which enable formate quantification but only in simple biochemical mixtures and/or with extensive sample processing/destruction. We envisioned that activity-based sensing (ABS), which leverages the intrinsic chemical reactivity of an analyte for its selective and sensitive detection,[13,14] could present a complementary strategy for formate analysis that is compatible with live cells and can provide spatiotemporal information regarding one-carbon metabolic flux.[13,14,15,16] As part of a growing field to discover and decipher the chemical roles that dynamic one-carbon metabolites play at a cellular level, our laboratory and others have developed ABS methods for carbon monoxide,[17,18,19] formaldehyde,[16,20,21,22,23,24,25,26,27] and carbon dioxide,[14,28] as well as related carbon signaling molecules such as ethylene.[29,30,31,32,33,34]

Here, we report an organometallic ABS method for detection of biological formate using a two-component system, where formate-mediated iridium transfer hydrogenation (TH) enables aldehyde-to-alcohol reduction on fluorophore scaffolds accompanied by a fluorescence response (Figure 1). Owing to its selectivity and sensitivity for this key one-carbon unit, this ABS system can monitor changes in endogenous formate levels in living cells, including in cell-based models of cancer with altered one-carbon metabolism.

RESULTS AND DISCUSSION

Design Considerations for Activity-Based Sensing of Formate Using a Transfer Hydrogenation Approach.

Activity-based sensing (ABS) methods achieve selectivity by judicious exploitation of the intrinsic reactivity of an analyte of interest for its detection, rather than traditional binding-based approaches that rely on lock-and-key molecular recognition.[13,14] This strategy is particularly attractive for detection of reactive small molecules in biological systems, such as reactive carbon species,[15,16,17,18,19,20,21,22,23,24,25,26,27,28,29,30,35] as these species are often transient and can interconvert between competing biological analytes of similar shape and size. In this regard, we recognized that formate is a hydride donor ($\Delta G°$=24.1 kcal/mol in H_2O).[36] This reactivity is illustrated by the Eschweiler-Clarke reaction,[37,38,39] its widespread use in transfer hydrogenation (TH) catalysis,[40] and its biochemical roles in regeneration of NADPH from $NADP^+$ via ALDH1L1/2 activity.[41] Therefore, we selected transfer hydrogenation as an ABS strategy for monitoring cellular formate fluxes (Figure 1). To this end, we sought to develop a two-component system for activity-based formate sensing comprised of a transfer hydrogenation metal-complex that uses formate as a reductant along with a fluorescent dye substrate that generates a fluorescence response upon its reduction. To achieve this goal of formate ABS, we sought to solve the following synthetic methods challenges: *1)* develop an appropriate fluorophore platform where reductive aldehyde-to-alcohol conversion would generate a measurable fluorescence response, *2)* identify a transition metal mediator for formate-mediated transfer hydrogenation that could operate with sufficiently high activity and robustness in the complex milieu of living cells, and *3)* tune the metal-complex/fluorophore pair so as to achieve biologically-relevant selectivity for formate over other potential cellular hydride sources[42,43] (e.g, NAD(P)H, 5,10-Me-THF, and $FADH_2$) and selectivity for the aldehydic fluorophore over other hydride acceptors, including electrophiles such as $NAD(P)^+$, carbonyls, *etc.*, and oxidants such as O_2, H_2O_2, *etc.* We discuss below how comprehensive screening experiments led to the selection and use of fluorophore **F-7** and complex **9** as a two-component system for enabling visualization of formate fluxes in living cells using confocal microscopy (Figure 2).

Fluorophore Development and Selection for Turn-On and Ratiometric Responses to Formate.

At the outset of our investigations, we sought to identify an aldehyde-containing fluorescent dye platform where formate-mediated reduction to the corresponding alcohol fluorophore would give an intensity-based turn-on response. In this context, the known aldehyde-containing fluorophore reported to have the highest intensity-based turn-on responses

upon aldehyde-to-alcohol reduction in the literature are **SI-1**,[44] a push-pull fluorophore, which provides a ~10x increase in emission intensity with aldehyde-to-alcohol reduction; however, this dye scaffold requires high-energy ultraviolet excitation at 300 nm. In terms of shifting optical responses to the visible excitation/emission region, which minimizes cellular autofluorescence and photodamage, the BODIPY fluorophore **SI-2**[45,46] achieves excitation at 480 nm but shows only a ~5x increase upon reduction (Table SI-1). We thus turned our attention to fluorescein-like xanthenone scaffolds, as rational principles for modulation of their fluorescence properties have been elucidated by Nagano and Urano.[47,48,49,50] In particular, we sought to employ a donor photoinduced electron transfer (dPeT) strategy to develop aldehyde dyes that would exhibit significant turn-on responses upon reduction to their alcohol congeners at lower energy visible excitation wavelengths (λ_{ex} ~500 nm).[47,48,49,50]

Based on the aforementioned reasoning, we calculated LUMO energy values for selected substituted benzaldehydes and then correlated these values with fluorescence quantum yields measured experimentally in previous reports.[47,48,50] This data-driven process identified aldehyde **F-1** and its corresponding alcohol **F-9** as a candidate pair for a turn-on dPeT fluorescence response (Figure 3). We then made two other considerations in selecting **F-1**. First, we placed the activity-based sensing aldehyde group at the *meta* position of the aromatic bottom ring to mitigate potential undesirable reactivity with cellular aldehyde dehydrogenases, which can react with *para* benzaldehydes.[51] Second, our calculations indicated that the hydrate form of **F-1**, designated as **F-8**, is also expected to be bright (Figure 3A), so an analysis correlating LUMO energy values with experimentally measured equilibrium values for substituted benzaldehyde-hydrate pairs was also conducted (Figure 3B).[52] This analysis predicted a 98.5 to 1.5 ratio between **F-1** and **F-8** in pH 7 water – sufficiently in favor of the aldehyde form to motivate synthetic efforts. Milligram quantities of fluorophore **F-1** were obtained in 7 steps from compound **20** (Figure 3C). Gratifyingly, we found that **F-9** provides an ~11-fold increase in emission intensity relative to **F-1** upon excitation at 500 nm under physiologically relevant aqueous conditions *in vitro* (pH 7.4 phosphate-buffered saline at 37 °C, Figure 4).

We employed fluorophore **F-1** for mediator evaluation and selectivity optimization studies *in vitro*, but this intensity-based scaffold did not provide reliable turn-on responses to formate in preliminary confocal imaging experiments (*vide infra*). Instead, we observed time- and formate-dependent decreases in fluorescence intensity, which we speculated may be due to fluorophore export and/or degradation from formate-stimulated production of ROS,[53] among other possibilities. As several attempts[54,55,56] to overcome this problem were ineffective, we sought to replace the intensity-responsive fluorophore **F-1** with a ratiometric fluorophore. We reasoned that this alternative approach would enable us to determine changes in formate concentrations based on the relative ratio of aldehyde/alcohol fluorophore species via two distinct excitation wavelengths with an internal self-calibration, rather than rely on the absolute intensity of emission of a mixture of fluorophores at a single wavelength. Indeed, two-color ratiometric measurements can minimize artifacts that can arise from variations in sample illumination and/or collection, non-homogeneous probe loading, changes in pH and probe localization, and fluorophore export and/or degradation.[20,57,58] Evaluation of several

types of dyes led us to aldehyde **F-7** and its corresponding alcohol form, **F-10** (Figure 5),[59,60] which display suitable excitation scan profiles (λ_{ex} = 400–500 nm respectively and λ_{em} = 510 nm) and sufficiently low steric hindrance about the aldehyde functional group to facilitate reduction by various transfer hydrogenation mediators, including Complex **9** (Figure 5). By comparison, aldehyde **F-2** required ultraviolet excitation at 300 nm, which is incompatible with live-cell imaging.[61] Likewise, reduction of **F-3**[62] resulted in a turn-off response, while dyes **F-4**[63] and **F-5**[64] not exhibit suitable ratiometric behavior. Finally, aldehyde **F-6**[65] underwent reduction more slowly than **F-7**[24] (Figure SI-5–9). Therefore, we employed fluorophore **F-7** in subsequent confocal microscopy imaging experiments (*vide infra*).

Metal-complex Development and Selection for Formate Activity and Selectivity.

Several classes of transfer hydrogenation (TH) mediators were evaluated using fluorophore **F-1** to identify a suitable metal-complex system for formate-mediated reduction of this aldehyde dye to its alcohol congener. Of the thousands of known transition metal TH catalysts,[40] we focused on a subset of iridium, osmium, and ruthenium complexes reported to engage in transfer hydrogenation under aqueous conditions (Figure 2B).[42,43,46,65,66,67,68,69,70,71] Most notable among these systems, the Do laboratory has reported an unprotected half-sandwich iridium complex, which can reduce the aldehydic BODIPY fluorophore **SI-2** (Table SI-1) in NIH 3T3 cells and proposed NADH as a hydride donor.[46]

Preliminary assessment of several of these complexes (**1**, **2**, **3**, **4**, **10** and **15** at 10 μM) showed that they could mediate the reduction of fluorophore **F-1** (10 μM) with sodium formate (100 μM) in phosphate buffered-saline (20 mM pH 7.4). Notably, we observed that the iridium complexes (complexes **4**, **10** & **15)** reduced fluorophore **F-1** about >30x faster than ruthenium **(1**) and osmium (**2**) complexes that bear similar ligands (Table SI-4). The one exception was iridium complex **3**, which is known to reduce molecular oxygen to hydrogen peroxide and did not reduce **F-1**.[72] Therefore, we focused our efforts on screening iridium complexes bearing bidentate N–N chelating ligands. We were gratified to find that iridium complexes bearing either pyridine amide[46] or sulfonamide amine ligands[65,69] reduce fluorophore **F-1** at 10 μM concentrations of **F-1** and metal complex in a formate-dependent manner, consistent with the previously observed first order rate dependence[66] on all three reactants.

To evaluate selectivity between biologically relevant hydride sources, representative iridium complexes **4** and **15** were initially surveyed *in vitro* for reduction of aldehyde **F-1** with NADH, NADPH, $FADH_2$ and 5,10-Me-THF.[43] These pilot experiments indicated that NAD(P)H, but not $FADH_2$ or 5,10-Me-THF, could present potential selectivity issues. Therefore, reduction of **F-1** was iteratively surveyed with an expanded set of metal complexes, **4**-**19**, using either sodium formate or NADH as a hydride source to reveal a generally strong rate preference for NADH over formate with pyridine amide complexes **4**-**7**, with modest NADH/formate selectivity for complexes **8** and **9**, which flips to a modest rate preference for formate over NADH for selected sulfonamide amine complexes **10**-**19** (Figure 6A).

We hypothesize that the more rapid hydride transfer observed for NADH over formate reflects a kinetic rather than thermodynamic preference, given that formate (ΔG°=24.1 kcal/mol in H_2O)[36] has more favorable endergonicity than NAD(P)H (ΔG°=28.9 kcal/mol in H_2O)[36] for hydride transfer.[74] We speculate that this kinetic difference may be due to *m*-amide coordination of the dihydropyridine moiety of NADH to the iridium center prior to hydride transfer via a 6-membered transition state,[75] whereas formate hydride transfer would have a more entropically challenging 4-membered, non-coordinating ion-paired, or 6-membered hydrogen bonded (via a pendant ligand N–H moiety) transition state.[40,76] Indeed, selectivity with a sulfonamide amine complex could be significantly improved to 2.7:1 in favor of formate by using a steric interaction at R^1 in the case of complex **19**, which may be due to a disfavorable 1,3-diaxial interaction between the benzyl group and NADH, which is not present with formate (Figure 6B).

Next, we conducted analyte selectivity assays to evaluate reduction of **F-1** using sulfonamide amine complex **19** and pyridine amide complex **9** with several biologically relevant endogenous hydride sources, reactive oxygen species (ROS), and reactive carbon species (RCS), including NAD(P)H, FADH, 5,10-Me-THF, formaldehyde, methanol, pyruvate, acetate, acrolein, glucose, hydrogen peroxide and hypochlorite (Figure 7A and 7B). In particular, we evaluated iridium complex **9** since it exhibited a 2.7-fold faster rate of reduction of **F-1** with sodium formate compared to complex **19** (Figure 7C and 7D), while also exhibiting the highest relative ratio of formate to NADH reactivity in the pyridine amide complex series (Figure 7A), presaging its potential for formate-dependent imaging in living cells using confocal microscopy (*vide infra)*.

Indeed, while promising *in vitro*, complex **19** exhibited low sensitivity to exogenously added sodium formate in preliminary live-cell confocal microscopy experiments (Figure SI-16), consistent with an *in vitro* assay showing strong inhibition of sulfonamide amine-type complex **19** to cellular thiols such as cysteine and glutathione (GSH) (Table SI-5). Overcoming the inhibitory activity of cellular thiols on transition metal catalysts is a challenging issue,[77,78] and while Ward and co-workers have designed protein-encapsulated iridium complexes that can sterically guard a sulfonamide amine iridium complex from inhibitory thiol chelation,[79] demonstration of this strategy in live cells remains elusive.[78] On the other hand, Do and colleagues have shown the capacity of half-sandwich pyridine amide complexes such as complex **9** to operate in live cells,[46,66,67] and *in vitro* assays showed that while aldehyde reduction in the presence of cellular thiols (GSH or cysteine) is slowed, TH reactivity with sodium formate, complex **9**, and fluorophore **F-1** is still operative (Table SI-5).

Activity-Based Imaging of Exogenous and Endogenous Formate Fluxes in Living Cells Using Transfer Hydrogenation.

Balancing factors of formate reactivity *in vitro* versus in the presence of biologically relevant cellular thiols, and taking selectivity for formate versus NADH into account, we therefore elected to use complex **9** over **19** for subsequent live-cell imaging experiments for formate detection. Although complex **9** is slightly more reactive to NAD(P)H over formate *in vitro* (Figure 7B), bioavailable formate concentrations far exceed those of bioavailable NAD(P)H.

Indeed, formate accumulates in mammalian blood in the range of 10–100 μM under physiological conditions[1] and reaches above 1 mM intracellularly.[6] In contrast, although estimates of the cellular NADPH (50–250 μM)[80] and NADH (100–200 μM) levels are lower or comparable to formate, the bioavailable pool is much lower, as 80% of mitochondrial NADH is estimated to be protein-bound rather than bioavailable.[81] Moreover, formate itself is a biochemical precursor to NAD(P)H, because formate is directly consumed by the enzymes ALDH1L1/2 to generate NADPH from $NADP^+$. Given these large differences in bioavailable biological concentrations between these hydride donors and that formate is a direct upstream source of NAD(P)H, we hypothesized that a combination of complex **9** and ratiometric fluorophore **F-7** would provide a suitable two-component system for activity-based imaging of formate pools in living cells.

To this end, we first evaluated the ability of **F-7** and complex **9** to visualize changes in formate levels in living cells upon exogenous addition of this one-carbon unit (Figure 8). We treated two types of representative mammalian cell lines, NIH 3T3 (mouse fibroblast) and HCT 116 (human colorectal carcinoma) cells, with **F-7** (10 μM) for 30 min followed by washing to remove excess fluorophore, with subsequent addition of metal-complex **9** (10 μM) for 60 min, followed by exposure to various concentrations of formate (50 μM to 500 μM). Visualization by live-cell imaging using confocal microscopy showed significant and dose-dependent ratiometic fluorescence changes in response to formate versus control cells (Figure 8), demonstrating the ability of complex **9** and fluorophore **F-7** to detect changes in exogenous formate levels in a cellular context.

We next investigated whether complex **9** and fluorophore **F-7** could be applied to image changes in endogenous formate fluxes based on nutrient-dependent alterations in one-carbon metabolism within the cell. First, we supplemented colon cancer HCT 116 wild-type (WT) cells with the native one-carbon donor serine (500 μM) for 60 min, washed, treated with fluorophore **F-7** (10 μM) for 30 min, washed, labeled with complex **9** (10 μM) for 60 min, and then imaged the formate-dependent ratiometric responses by confocal microscopy. We observed a significant increase in the reduction of aldehyde **F-7** to its alcohol counterpart **F-10**, indicating elevated levels of cellular formate and NAD(P)H in serine-supplemented cells relative to vehicle-treated controls (Figure 9B). This result is consistent with our expectations because excess serine may be metabolized to form up to 2 equivalents of NAD(P)H and 1 equivalent of formate (Figure 9A–C) in one-carbon metabolic cycles.[1,2,3,4] Specifically, excess cellular serine may be metabolized to glycine and 5,10-methylene-tetrahydrofolate (5,10-CH_2-THF) through the activity of SHMT1/2 (cytosolic and mitochondrial isoforms), while 5,10-CH_2-THF may be oxidized to 10-formyl-tetrahydrofolate (10-CHO-THF) via MTHFD1 or MTHFD2/2L and then to formate/formic acid after spontaneous or enzymatic hydrolysis via MTHFD or MTHFD1L. Alternatively, 5,10-CH_2-THF can spontaneously release formaldehyde,[23] which can be oxidized directly to formate by ALDH2 and/or scavenged by glutathione (GSH) and oxidized to *S*-formylglutathione (GS-CHO) by ADH5; GS-CHO releases formate upon hydrolysis (Figure 9A).

With these results in hand, we sought to further decipher formate-generating pathways in the cell by activity-based imaging using colon cancer cell lines with genetic alterations

in key one-carbon metabolism enzymes. Specifically, we conducted comparative imaging experiments with HCT116 wild-type (WT) cells and HCT116 lines with a *SHMT1/SHMT2/ADH5* triple knockout (tKO). *SHMT1/2* double knockout HCT 116 cells have impaired serine consumption, blocking the predominant source of formate.[82,83] And since formaldehyde can be an additional source of formate to support one-carbon units in the absence of SHMT1/2, we also tested cells with an additional *ADH5* knock out to further deplete basal cellular formate pools.[84] We used our standard imaging protocol (10 μM **F-7** for 30 min, wash, 10 μM complex **9** for 60 min, wash, then imaging by confocal microscopy) to see the effect of removing enzymes upstream of formate/NAD(P)H production (Figure 9A). Gratifyingly, we observed a significant decrease in iridium-mediated ratiometric responses in the tKO HCT 116 cells (cells lacking *SHMT1, SHMT2*, and *ADH5*) relative to the wild-type controls, indicating deficient formate production by blocking multiple one-carbon metabolism pathway inputs in parallel (Figure 9C).

CONCLUDING REMARKS

To close, we have presented a transfer hydrogenation (TH) approach to activity-based sensing (ABS) of formate in living cells. We have developed a two-component ABS system consisting of a metal complex and fluorescent dye, in which the metal complex utilizes formate as a reductant to mediate the conversion of an aldehyde-functionalized fluorescent dye to its alcohol counterpart with a concomitant fluorescence response. Owing to the generality of this ABS approach, and in particular the flexibility of mixing and matching metal-complex and dye components to tune fluorescence outputs, we have developed formate reporter systems that operate using either an intensity-based turn-on response with a single excitation/emission signature or a ratiometric response with a dual excitation/emission shift for self-calibration, respectively. In-depth evaluation of electron transfer properties in fluorescein-like fluorophore scaffolds afforded a pair of dyes where formate-mediated aldehyde-to-alcohol conversion gave a significant 11-fold fluorescence turn-on response, which was then used to systematically screen several classes of iridium complexes for optimizing formate-mediated transfer hydrogenation in aqueous solution. Despite the aforementioned benefits based on the modularity of this ABS formate detection system, it is multi-component and requires the colocalization of the metal-hydride complex and the fluorogenic substrate. Further development towards systems that reduce the number of components could improve the sensitivity of metal-hydride transfer chemistry for formate sensing in live cells and more complex biological specimens.

To advance this formate ABS platform from *in vitro* assays to live-cell imaging applications, we developed coumarin aldehyde fluorophore **F-7**, which was utilized alongside iridium complex **9** to achieve a robust ratiometric fluorescence response to physiologically relevant concentrations of formate as well as selectivity over potentially competing analytes through iridium- and formate-mediated conversion of aldehyde dye **F-7** to its alcohol congener **F-10**. We then established that this formate ABS system is capable of detecting changes in intracellular formate levels with exogenous formate addition. Furthermore, we showed that this ABS platform is sufficiently sensitive to monitor changes in basal formate fluxes in a cell-based model of human colorectal cancer, where genetic knockout of amino

acid (serine) and formaldehyde scavenging (ADH5) biochemical pathways for endogenous formate production result in formate deficiency. Future work will explore the application of this two-component system for studying contributions of formate as a one-carbon metabolite in cancer and neurodegenerative diseases. In addition to providing a unique chemical tool for deciphering biological contributions of formate, this study provides a starting point for the broader adoption of organometallic chemistry in the design of activity-based sensing probes and related reagents for chemical biology.

Supplementary Material

Refer to Web version on PubMed Central for supplementary material.

ACKNOWLEDGMENT

We thank Alison Killilea (UC Berkeley Tissue Culture Facility) for expert technical assistance and Hasan Celik, Alicia Lund, and UC Berkeley's NMR facility in the College of Chemistry (CoC-NMR) for spectroscopic assistance. Prof. Nathan Schley is thanked for helpful discussion. We thank Profs. J. D. Rabinowitz and K. J. Patel for sharing the HCT 116 wild-type, *SHMT1/SHMT2* double knockout, and *SHMT1/SHMT2/ADH5* triple knockout cell lines.

Funding Sources

We thank the NIH (ES 28096 and GM 139245 to C.J.C.) for support of this work. S.W.M.C. was supported by the AGBT-Elaine R. Mardis Fellowship in Cancer Genomics from the Damon Runyon Cancer Research Foundation and The Genome Partnership, Inc. (DRG-2395-20). V.N.P. was supported by the National Science Foundation for Graduate Research Fellowship and NIH Chemical Biology Interface Training Grant T32 GM066698. X.X. was supported as a Tang Foundation Distinguished Scholar (UC Berkeley QB3). C.J.C. is a CIFAR Fellow. Instruments in the CoC-NMR are supported in part by NIH S10OD024998.

ABBREVIATIONS

ADH5	alcohol dehydrogenase 5
ALDH2	aldehyde dehydrogenase 2
MTHFD1L	methylenetetrahydrofolate dehydrogenase (NADP+ dependent) 1 like
ALDH1L1/2	aldehyde dehydrogenase family member L1 & L2
THF	tetrahydrofolate; 10-CHO-THF, 10-formyl-tetrahydrofolate
NAD(P)H	nicotinamide adenine dinucleotide (phosphate)
$FADH_2$	flavin adenine dinucleotide
5,10-CH_2-THF	5,10-methylene-tetrahydrofolate
TLC	thin layer chromatography

REFERENCES

1. Pietzke M; Meiser J; Vazquez A, Formate metabolism in health and disease. Mol. Metab 2020, 33, 23–37. [PubMed: 31402327]

2. Brosnan ME; Brosnan JT, Formate: The neglected member of one-carbon metabolism. Ann. Rev. Nutr 2016, 36(1), 369–388. [PubMed: 27431368]
3. Ducker GS; Rabinowitz JD, One-carbon metabolism in health and disease. Cell Metab 2017, 25(1), 27–42. [PubMed: 27641100]
4. Newman AC; Maddocks ODK, One-carbon metabolism in cancer. Br. J. Cancer 2017, 116(12), 1499–1504. [PubMed: 28472819]
5. Oizel K; Tait-Mulder J; Fernandez-de-Cossio-Diaz J; Pietzke M; Brunton H; Lilla S; Dhayade S; Athineos D; Blanco GR; Sumpton D; Mackay GM; Blyth K; Zanivan SR; Meiser J; Vazquez A, Formate induces a metabolic switch in nucleotide and energy metabolism. Cell Death Dis 2020, 11 (5), 310–324. [PubMed: 32366892]
6. 10–50% of formaldehyde (20–100 μM in blood; 200–500 μM intracellularly) in mammalian cells is converted into formate. SeeTong Z; Han C; Luo W; Wang X; Li H; Luo H; Zhou J; Qi J; He R, Accumulated hippocampal formaldehyde induces age-dependent memory decline. Age 2013, 583, 596.;Burgos-Barragan G; Wit N; Meiser J; Dingler FA; Pietzke M; Mulderrig L; Pontel LB; Rosado IV; Brewer TF; Cordell RL; Monks PS; Chang CJ; Vazquez A; Patel K, Mammals divert endogenous genotoxic formaldehyde into one-carbon metabolism. Nature 2017, 548(7669), 549–554.; [PubMed: 28813411] The half-saturation for formate efflux from human erythrocytes is 9 mM.[1,5].
7. Wang Y; Wang Y; Zhu J; Guan Y; Xie F; Cai X; Deng J; Wei Y; He R; Fang Z; Guo Q, Systematic evaluation of urinary formic acid as a new potential biomarker for alzheimer's disease. Front. Aging Neurosci 2022, 14(1046066), 1–12.
8. Meiser J; Schuster A; Pietzke M; Voorde JV; Athineos D; Oizel K; Burgos-Barragan G; Wit N; Dhayade S; Morton JP; Dornier E; Sumpton D; Mackay GM; Blyth K; Patel KJ; Niclou SP; Vazquez., Increased formate overflow is a hallmark of oxidative cancer. Nature Comm 2018, 9(1), 1368–1380.
9. Wang L; Chen J; Chen L; Deng P; bu Q; Xiang P; Li M; Lu W; Xu Y; Lin H; Wu T; Wang H; Hu J; Shao X; Cen X; Zhao Y-L, 1H-NMR based metabonomic profiling of human esophageal cancer tissue. Mol. Cancer 2013, 12 (1), 25–39. [PubMed: 23556477]
10. Whitteck JT; Cicchillo RM; van der Donk WA, Hydroperoxylation by hydroxyethylphosphonate dioxygenase. J. Am. Chem. Soc 2009, 131, 16225–16232. [PubMed: 19839620]
11. Warui DM; Li N; Nørgaard H; Krebs C; Bollinger JM Jr.; Booker SJ, Detection of formate, rather than carbon monoxide, as the stoichiometric coproduct in conversion of fatty aldehydes to alkanes by a cyanobacterial aldehyde decarbonylase. J. Am. Chem. Soc 2011, 133, 3316–3319. [PubMed: 21341652]
12. Formate Assay Kit; MAK059–1KT; Sigma-Aldrich: St. Louis, MO, October 24, 2023. https://www.sigmaaldrich.com/deepweb/assets/sigmaaldrich/product/documents/274/457/mak059bul.pdf (accessed 2024-02-26).
13. Chan J; Dodani SC; Chang CJ, Reaction-based small-molecule fluorescent probes for chemoselective bioimaging. Nature Chem 2012, 4, 973–984. [PubMed: 23174976]
14. Bruemmer KJ; Crossley SWM; Chang CJ, Activity-based sensing: A synthetic methods approach for selective molecular imaging and beyond. Angew. Chem. Int. Ed. Engl 2020, 59(33), 13734–13762. [PubMed: 31605413]
15. Ohata J; Bruemmer KJ; Chang CJ, Activity-based sensing methods for monitoring the reactive carbon species carbon monoxide and formaldehyde in living systems. Acc. Chem. Res 2019, 52(10), 2841–2848. [PubMed: 31487154]
16. Bruemmer KJ; Brewer TF; Chang CJ, Fluorescent probes for imaging formaldehyde in biological systems. Curr. Opin. Chem. Biol 2017, 39, 17–23. [PubMed: 28527906]
17. Ueno K; Morstein J; Ofusa K; Naganos S; Suzuki-Sawano E; Minegishi S; Rezgui SP; Kitagishi H; Michel BW; Chang CJ; Horiuchi J; Saitoe M, Carbon monoxide, a retrograde messenger generated in postsynaptic mushroom body neurons, evokes noncanonical dopamine release. J. Neurosci 2020, 40(18), 3533–3548. [PubMed: 32253360]
18. Michel BW; Lippert AR; Chang CJ, A reaction-based fluorescent probe for selective imaging of carbon monoxide in living cells using a palladium-mediated carbonylation. J. Am. Chem. Soc 2012, 134(38), 15668–15671. [PubMed: 22970765]

19. Morstein J; Höfler D; Ueno K; Jurss JW; Walvoord RR; Bruemmer KJ; Rezgui SP; Brewer TF; Saitoe M; Michel BW; Chang CJ, Ligand-directed approach to activity-based sensing: developing palladacycle fluorescent probes that enable endogenous carbon monoxide detection. J. Am. Chem. Soc 2020, 142(37), 15917–15930. [PubMed: 32872768]
20. Brewer TF; Chang CJ, An aza-Cope reactivity-based fluorescent probe for imaging formaldehyde in living cells. J. Am. Chem. Soc 2015, 137(34), 10886–10889. [PubMed: 26306005]
21. Roth A; Li H; Anorma C; Chan J, A reaction-based fluorescent probe for imaging of formaldehyde in living cells. J. Am. Chem. Soc 2015, 137, 10890–10893. [PubMed: 26305899]
22. Bruemmer KJ; Walvoord RR; Brewer TF; Burgos-Barragan G; Wit N; Pontel LB; Patel KJ; Chang CJ, Development of a general aza-Cope reaction trigger applied to fluorescence imaging of formaldehyde in living cells. J. Am. Chem. Soc 2017, 139(15), 5338–5350. [PubMed: 28375637]
23. Burgos-Barragan G; Wit N; Meiser J; Dingler FA; Pietzke M; Mulderrig L; Pontel LB; Rosado IV; Brewer TF; Cordell RL; Monks PS; Chang CJ; Vazquez A; Patel KJ, Mammals divert endogenous genotoxic formaldehyde into one-carbon metabolism. Nature 2017, 548(7669), 549–554. [PubMed: 28813411]
24. Brewer TF; Burgos-Barragan G; Wit N; Patel KJ; Chang CJ, A 2-aza-Cope reactivity-based platform for ratiometric fluorescence imaging of formaldehyde in living cells. Chem. Sci 2017, 8(5), 4073–4081. [PubMed: 28580121]
25. Bruemmer KJ; Green O; Su TA; Shabat D; Chang CJ, Chemiluminescent probes for activity-based sensing of formaldehyde released from folate degradation in living mice. Angew. Chem. Int. Ed. Engl 2018, 57(25), 7508–7512. [PubMed: 29635731]
26. Smaga LP; Pino NW; Ibarra GE; Krishnamurthy V; Chan J, A photoactivatable formaldehyde donor with fluorescence monitoring reveals threshold to arrest cell migration. J. Am. Chem. Soc 2020, 142(2), 680–684. [PubMed: 31898899]
27. Toh JDW; Crossley SWM; Bruemmer KJ; Ge EJ; He D; Iovan DA; Chang CJ, Distinct RNA N-demethylation pathways catalyzed by nonheme iron ALKBH5 and FTO enzymes enable regulation of formaldehyde release rates. Proc. Natl. Acad. Sci. U.S.A 2020, 117(41), 25284–25292. [PubMed: 32989163]
28. Green O; Finkelstein P; Rivero-Crespo MA; Lutz MDR; Bogdos MK; Burger M; Leroux JC; Morandi B, Activity-based approach for selective molecular CO_2 sensing. J. Am. Chem. Soc 2022, 144(19), 8717–8724. [PubMed: 35503368]
29. Toussaint SNW; Calkins RT; Lee S; Michel BW, Olefin Metathesis-Based Fluorescent Probes for the Selective Detection of Ethylene in Live Cells. J. Am. Chem. Soc 2018, 140, 13151–13155. [PubMed: 30281288]
30. Jensen KH; Michel BW, Detection of Ethylene with Defined Metal Complexes: Strategies and Recent Advances, Analysis & Sensing 2023, 3, e202200058. [PubMed: 37601898]
31. Ishihara S; Bahuguna A; Kumar S; Krishnan V; Labuta J; Nakanishi T; Tanaka T; Kataura H; Kon Y; Hong D, Cascade Reaction-Based Chemiresistive Array for Ethylene Sensing. ACS Sensors 2020, 5 (5), 1405–1410. [PubMed: 32390438]
32. Fong D; Luo S-XL; Andre RS; Swager TM, Trace Ethylene Sensing via Wacker Oxidation. ACS Central Sci 2020, 6 (4), 507–512.
33. Chen Y; Yan W; Guo D; Li Y; Li J; Liu H; Wei L; Yu N; Wang B; Zheng Y; Jing M; Zhao J; Ye Y, An Activity-Based Sensing Fluorogenic Probe for Monitoring Ethylene in Living Cells and Plants. Angew. Chem. Int. Ed 2021, 60(40), 21934–21942.
34. Vong K; Eda S; Kadota Y; Nasibullin I; Wakatake T; Yokoshima S; Shirasu K; Tanaka KAn artificial metalloenzyme biosensor can detect ethylene gas in fruits and Arabidopsis leaves. Nature Comm 2019, 10 (1), 5746.
35. Jana RD; Ngo AH; Bose S; Do LH, Organoiridium Complexes Enhance Cellular Defense Against Reactive Aldehyde Species. Chem. – Eur. J 2023, 29 (36), e202300842. 10.1002/chem.202300842.). [PubMed: 37058398]
36. Connelly SJ; Wiedner ES; Appel AM, Predicting the reactivity of hydride donors in water: Thermodynamic constants for hydrogen. Dalton Trans 2015, 44, 5933–5938. [PubMed: 25697077]
37. Eschweiler W, Ersatz von an Stickstoff gebundenen Wasserstoffatomen durch die Methylgruppe mit Hülfe von Formaldehyd. Ber 1905, 38, 880–882. doi:10.1002/cber.190503801154.

38. Clarke HT; Gillespie HB; Weisshaus SZ, The action of formaldehyde on amines and amino acids. J. Am. Chem. Soc 1933, 55(11), 4571–4587.
39. Pine SH; Sanchez BL, Formic acid-formaldehyde methylation of amines. J. Org. Chem 1971, 36(6), 829–832.
40. Wang D; Astruc D, The golden age of transfer hydrogenation. Chem. Rev 2015, 115, 6621–6686. [PubMed: 26061159]
41. Xiao W; Wang RS; Handy DE; Loscalzo J, NAD(H) and NADP(H) redox couples and cellular energy metabolism. Antioxid. Redox Signal 2018, 28(3), 251–272. [PubMed: 28648096]
42. Nguyen DP; Nguyen HTH; Do LH, Tools and methods for investigating synthetic metal-catalyzed reactions in living cells. ACS Catal 2021, 11, 5148–5165. [PubMed: 34824879]
43. Banerjee S; Sadler PJ, Transfer hydrogenation catalysis in cells. RSC Chem. Biol 2021, 2, 12–29. [PubMed: 34458774]
44. Guo H-M; Tanaka F, A fluorogenic aldehyde bearing a 1,2,3-triazole moiety for monitoring the progress of aldol reactions. J. Org. Chem 2009, 74, 2417–2424. [PubMed: 19222210]
45. Yue Y; Guo Y; Xu J; Shao S, A BODIPY-based derivative for selective fluorescence sensing of homocysteine and cysteine. New J. Chem 2011, 35, 61–64
46. Bose S; Ngo AH; Do LH, Intracellular transfer hydrogenation mediated by unprotected organoiridium catalysts. J. Am. Chem. Soc 2017, 139(26), 8792–8795. [PubMed: 28613857]
47. Nagano T, Development of fluorescent probes for bioimaging applications. Proc. Jpn. Acad., Ser. B, Phys 2010, 86 (8), 837–847.
48. Urano Y; Makiya M; Kanda K; Ueno T; Nagano T, Evolution of fluorescein as a platform for finely tunable fluorescence probes. J. Am. Chem. Soc 2005, 127(13), 4888–4894. [PubMed: 15796553]
49. Ueno T; Urano Y; Setsukinai K; Takakusa H; Kojima H; Kikuchi K; Ohkubo K; Fukuzumi S; Nagano T, Rational principles for modulating fluorescence properties of fluorescein. J. Am. Chem. Soc 2004, 126(43), 14079–14085. [PubMed: 15506772]
50. Tanaka K; Miura T; Umezawa N; Urano Y; Kikuchi K; Higuchi T; Nagano T, Rational design of fluorescein-based fluorescence probes, mechanism-based design of a maximum fluorescence probe for singlet oxygen. J. Am. Chem. Soc 2001, 123(11), 2530–2536. [PubMed: 11456921]
51. Anorma C; Hedhli J; Bearrood TE; Pino NW; Gardner SH; Inaba H; Zhang P; Li Y; Feng D; Dibrell SE; Kilian KA; Dobrucki LW; Fan TM; Chan J, Surveillance of cancer stem cell plasticity using an isoform-selective fluorescent probe for aldehyde dehydrogenase 1A1. ACS Cent. Sci 2018, 4, 1045–1055. [PubMed: 30159402]
52. Aldehyde-hydrate equilibrium values: McLelland RA; Coe M, Structure-reactivity effects in the hydration of benzaldehydes. J. Am. Chem. Soc 1983, 105, 2718–2725.
53. Young A; Gardiner D; Brosnan ME; Brosnan JT; Mailloux RJ, Physiological levels of formate activate mitochondrial superoxide/hydrogen peroxide release from mouse liver mitochondria. FEBS Letters 2017, 591(16), 2426–2438. [PubMed: 28771687]
54. Jansen ABA; Russell TJ, 379. Some novel penicillin derivatives. J. Chem. Soc, 1965, 2127–2132. [PubMed: 14288328]
55. Tsien RY, A non-disruptive technique for loading calcium buffers and indicators into cells. Nature 1981, 290, 527–528. [PubMed: 7219539]
56. Lavis LD, Live and let dye. Biochemistry 2021, 60(46), 3539–3546. [PubMed: 34096721]
57. Tsien RY, Fluorescence measurement and photochemical manipulation of cytosolic free calcium. Trends Neurosci, 1988, 11, 419–424. [PubMed: 2469158]
58. Lee MH; Kim JS; Sessler JL, Small molecule-based ratiometric fluorescence probes for cations, anions, and biomolecules. Chem. Soc. Rev 2015, 44, 4185–4191. [PubMed: 25286013]
59. Kirpichenok MA; Bakulev VM; Karandashova LA; Grandberg II, Synthesis and spectral and luminescent properties of 3-formyl-7-dialkylaminocoumarins. Chem. Heterocycl. Cmpnd 1991, 27, 1193–1199.
60. Beck MW; Kathayat RS; Cham CM; Chang EB; Dickinson Bryan C., Michael addition-based probes for ratiometric fluorescence imaging of protein *S*-depalmitoylases in live cells and tissues. Chem. Sci 2017, 8(11), 7588–7592. [PubMed: 29568422]

61. He L; Yang X; Liu Y; Kong X; Lin W, A ratiometric fluorescent formaldehyde probe for bioimaging applications. Chem. Commun 2016, 52, 4029–4032.
62. Petit M; Tran C; Roger T; Gallavardin T; Dhimane H; Palma-Cerda F; Blanchard-Desce M; Acher FC; Ogden D; Dalko PI, Substitution effect on one- and two-photon sensitivity of DMAQ “caging” groups. Org. Lett 2012, 14, 6366–6369. [PubMed: 23214948]
63. Yuan L; Lin W; Song J; Yang Y, Development of an ICT-based ratiometric probe suitable for living cell imaging. Chem. Comm 2011, 47, 12691–12693. [PubMed: 22037995]
64. Zhang P; Liu W; Niu G; Xiao H; Wang M; Ge J; Wu J; Zhang H; Li Y; Wang P, Coumarin-based boron complexes with aggregation-induced emission. J. Org. Chem, 2017, 82, 3456–3462. [PubMed: 28272896]
65. Letko CS; Heiden ZM; Rauchfuss TB, Activation and Deactivation of Cp* Ir (TsDPEN) Hydrogenation Catalysts in Water. Eur. J. Chem 2009, 33, 4927–4930.
66. Ngo AH; Do LH, Structure-activity relationship study of half-sandwich metal complexes in aqueous transfer hydrogenation catalysis. Inorg. Chem. Front 2020, 7(3), 583–591.
67. Ngo AH; Ibañez M; Do LH, Catalytic hydrogenation of cytotoxic aldehydes using nicotinamide adenine dinucleotide (NADH) in cell growth media. ACS Catal 2016, 6, 2637–2641.
68. Wu X; Liu J; Li X; Zanotti-Gerosa A; Hancock F; Vinci D; Ruan J; Xiao J, On water and in air: Fast and highly chemoselective transfer hydrogenation of aldehydes with iridium catalysts. Angew. Chem. Int. Ed 2006, 45, 6718–6722.
69. Wu X; Corcoran C; Yang S; Xiao J, A versatile iridium catalyst for aldehyde reduction in water. ChemSusChem Chem. Sustain. Energy Mater 2008, 1, 71–74.
70. Coverdale JPC; Romero-Canelón I; Sanchez-Cano C; Clarkson GJ; Habtemariam A; Wills M; Sadler PJ, Asymmetric transfer hydrogenation by synthetic catalysts in cancer cells. Nat. Chem 2018, 10(3), 347–354. [PubMed: 29461524]
71. Soldevila-Barreda JJ; Romero-Canlón I; Sanchez-Cano C; Clackson GJ; Habtemariam A; Wills M; Sadler PJ, Asymmetric hydrogenation by synthetic catalysts in cancer cells. Nat. Chem 2018, 10(3), 347–354. [PubMed: 29461524]
72. Liu Z; Romero-Canelón I; Qamar B; Hearn JM; Habtemariam A; Barry NPE; Pizarro AM; Clarkson GJ; Sadler PJ, The potent oxidant anticancer activity of organoiridium catalysts. Angew. Chem. Int. Ed 2014, 53, 3941–3946.
73. Pitman CL; Finster ONL; Miller AJM, Cyclopentadiene-mediated hydride transfer from rhodium complexes. Chem. Commun 2016, 52, 9105–9108.
74. Wiedner ES; Chambers MB; Pitman CL; Bullock RM; Miller AJM; Appel AM, Thermodynamic hydricity of transition metal hydrides. Chem. Rev 2016, 116(15), 8655–8692. [PubMed: 27483171]
75. Betanzos-Lara S; Liu Z; Habtemariam A; Pizarro AM; Qamar B; Sadler PJ, Organometallic ruthenium and iridium transfer-hydrogenation catalysts using coenzyme NADH as a cofactor. Angew. Chem. Int. Ed 2012, 51, 3897–3900.
76. Mwansa JM; Page MI, Catalysis, kinetics and mechanisms of organo-iridium enantioselective hydrogenation-reduction. Catal. Sci. Technol 2020, 10, 590–612.
77. Nguyen HD; Do LH Taming glutathione potentiates metallodrug action. Curr. Opin. Chem. Biol 2022, 71, 102213–102230. [PubMed: 36206677]
78. Soldevila-Barreda JJ; Metzler-Nolte N, Intracellular catalysis with selected metal complexes and metallic nanoparticles: Advances toward the development of catalytic metallodrugs. Chem. Rev 2019 119(2), 829–869. [PubMed: 30618246]
79. Liang AD; Serrano-Plana J; Peterson RL; Ward TR, Artificial metalloenzymes based on the biotin-streptavidin technology: Enzymatic cascades and directed evolution. Acc. Chem. Res 2019, 52(3), 585–595. [PubMed: 30735358]
80. Lu W; Wang L; Chen L; Hui S; Rabinowitz JD, Extraction and quantitation of nicotinamide adenine dinucleotide redox cofactors. Antioxid. Redox Signal 2018, 28(3), 167–179. [PubMed: 28497978]
81. Blinova K; Carroll S; Bose S; Smirnov AV; Harvey JJ; Knutson JR; Balaban RS, Distribution of mitochondrial NADH fluorescence lifetimes: Steady-state kinetics of matrix NADH interactions. Biochemistry 2005, 44(7), 2585–2594. [PubMed: 15709771]

82. Ducker GS; Chen L; Morscher RJ; Ghergurovich JM; Esposito M; Teng X; Kang Y; Rabinowitz JD Reversal of Cytosolic One-Carbon Flux Compensates for Loss of the Mitochondrial Folate Pathway. Cell Metabolism 2016, 23 (6), 1140–1153. [PubMed: 27211901]

83. Ducker GS; Ghergurovich JM; Mainolfi N; Suri V; Jeong SK; Hsin-Jung Li S; Friedman A; Manfredi MG; Gitai Z; Kim H; Rabinowitz JD Human SHMT Inhibitors Reveal Defective Glycine Import as a Targetable Metabolic Vulnerability of Diffuse Large B-Cell Lymphoma. Proceedings of the National Academy of Sciences 2017, 114 (43), 11404–11409.

84. Wit N; Gogola E; West JA; Vornbäumen T; Seear RV; Bailey PSJ; Burgos-Barragan G; Wang M; Krawczyk P; Huberts DHEW; Gergely F; Matheson NJ; Kaser A; Nathan JA; Patel KJ A Histone Deacetylase 3 and Mitochondrial Complex I Axis Regulates Toxic Formaldehyde Production. Science Advances 2023, 9 (20), eadg2235.

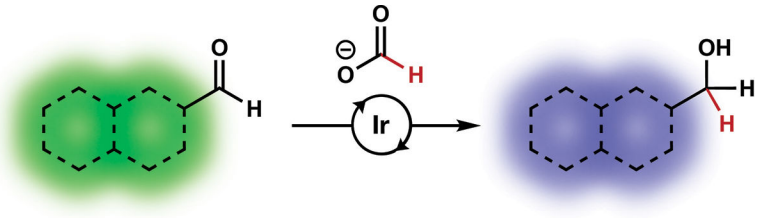

Figure 1.

Activity-based sensing (ABS) design strategy for cellular formate detection and imaging. Formate-mediated iridium transfer hydrogenation (TH) converts an aldehyde-linked fluorophore to an alcohol-linked fluorophore with a concomitant fluorescence response.

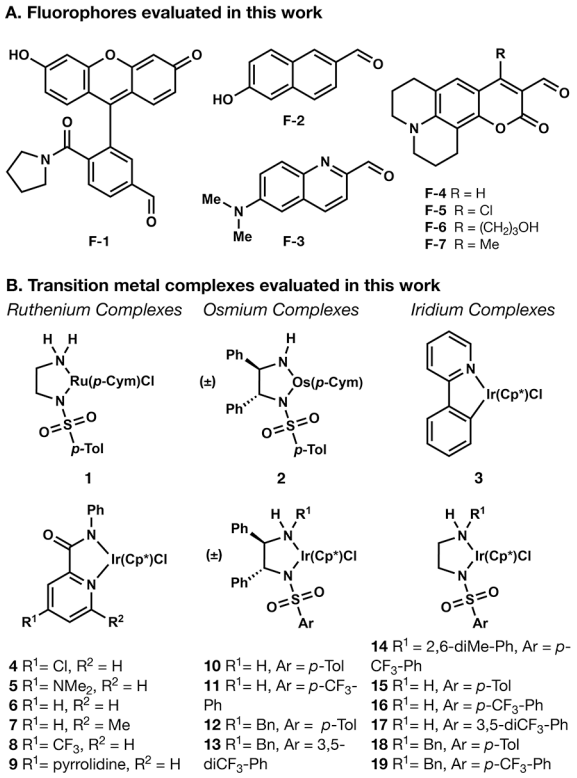

Figure 2.

(A) Fluorophores and (B) transition metal complexes evaluated in this work to develop activity-based formate sensors.

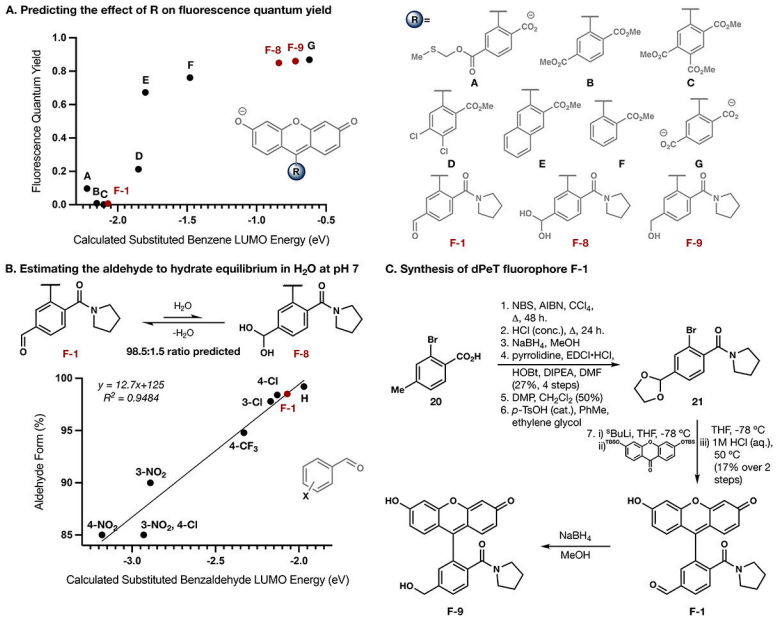

Figure 3.

Design, properties, and synthesis of a donor photoinduced electron transfer (dPeT) aldehyde fluorophore (**F-1**), where its formate-dependent metal-mediated reduction to alcohol **F-9** is accompanied by an intensity-based turn-on fluorescence response. (A) Correlations between experimentally measured fluorescence quantum yields (black dots) and calculated LUMO energy levels were used to predict candidate R groups (red dots) on fluorescein-like dyes with dim aldehyde forms and bright alcohol forms. (B) A linear correlation between experimentally measured substituted benzaldehyde-to-hydrate equilibria and the calculated substituted benzaldehyde LUMO energy value yields an estimated 98.5 to 1.5 ratio beween aldehyde (**F-1**) and hydrate (**F-8**). (C) Synthetic route to prepare dPeT fluorophore (**F-1**).

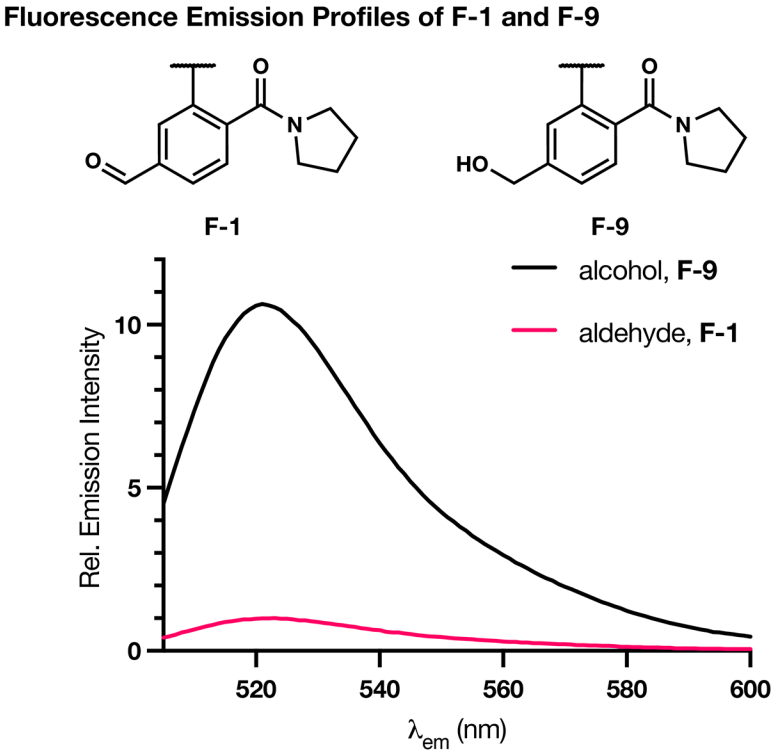

Figure 4.

Emission properties of aldehyde (**F-1**) and alcohol (**F-9**) dyes at 10 μM measured in 20 mM PBS, pH 7.4, with λ_{ex} = 500 nm.

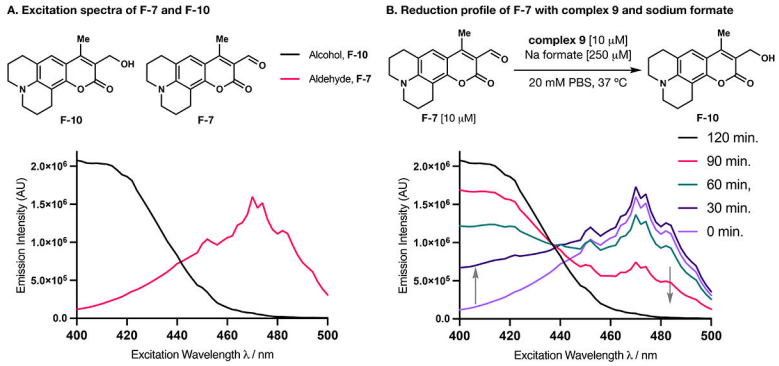

Figure 5.

(A) Excitation scans of alcohol dye **F-10** and aldehyde dye **F-7**. Data were acquired with 10 mM of fluorophore at 37 °C in 20 mM PBS (pH 7.4). Excitation spectra were collected between 400 and 500 nm with emission monitored at 510 nm.

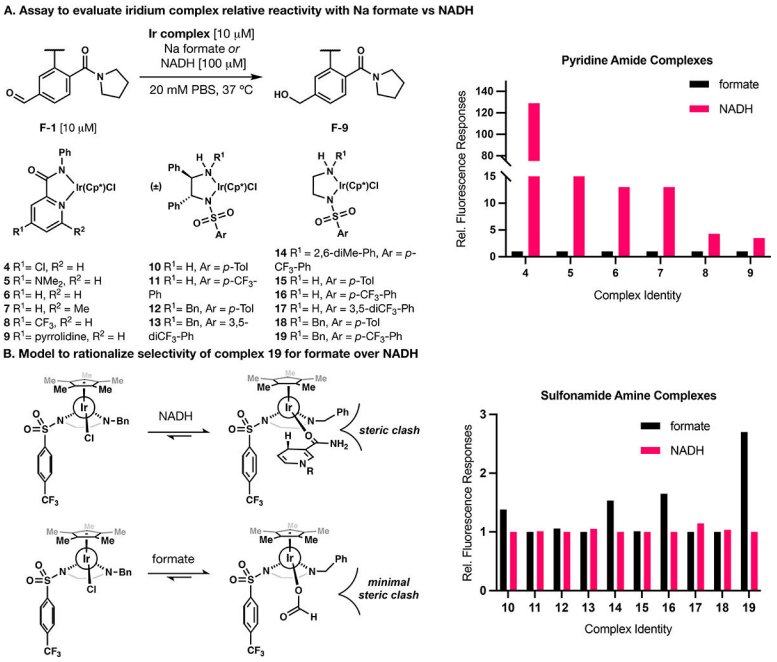

Figure 6.

(A) Effects of ligand structure on iridium complex selectivity for formate vs NADH as hydride donors for transfer hydrogenation. Systematic screening efforts used aldehyde and Ir complex ([10 μM] each) in 20 mM PBS (pH 7.4) at 37 °C. Fluorogenic reactions were monitored with λ_{ex} = 500 nm and λ_{em} = 510–600 nm. The relative fluorescence responses were measured based on the increase in fluorescence emission intensity at 522 nm between t = 0 and t = 30 min. (B) Proposed model for observation of higher selectivity for formate over NADH mediated by complex **19**, due to a disfavorable steric interaction with NADH.

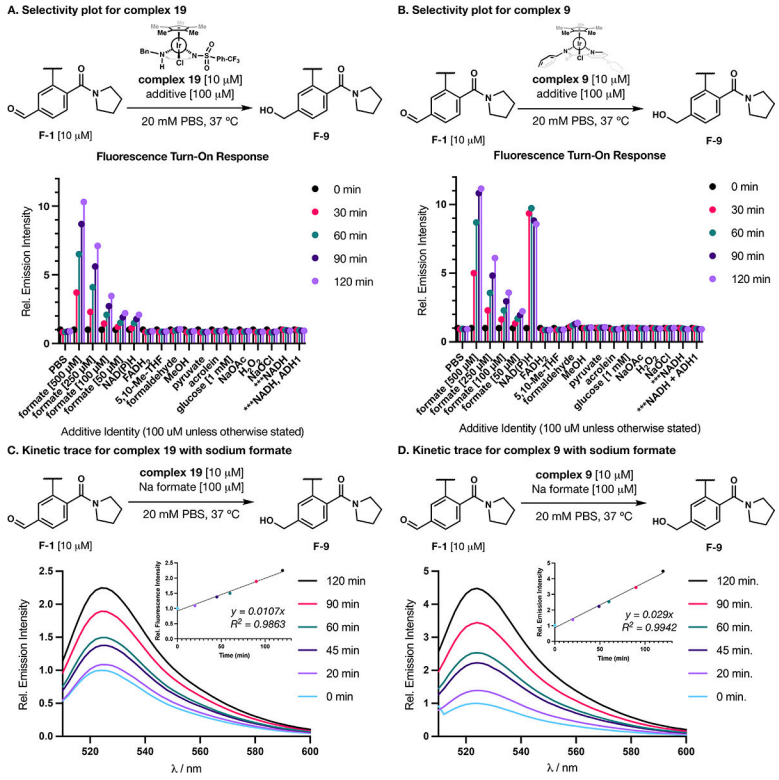

Figure 7.

(A) and (B) Fluorescence turn-on responses of fluorophore **F-1** [10 μM] to transfer hydrogenation by iridium complexes **19** and **9** [10 μM] in response to various biologically relevant hydride sources, reactive carbon species (RCS), and reactive oxygen species (ROS) (at 100 μM unless otherwise stated. ***The last two samples do not contain the Ir-complex, instead reactivity with ADH1 is assessed.) (C) and (D) Fluorescence responses of **F-1** [10 μM] to complexes **19** and **9** [10 μM] and sodium formate [100 μM]. Data were acquired at 37 °C in 20 mM PBS (pH 7.4) with excitation at λ_{ex} = 500 nm. Emission spectra were collected between 510 and 600 nm. Time points represent 0, 20, 45, 60, 90, and 120 min after addition of 100 μM sodium formate.

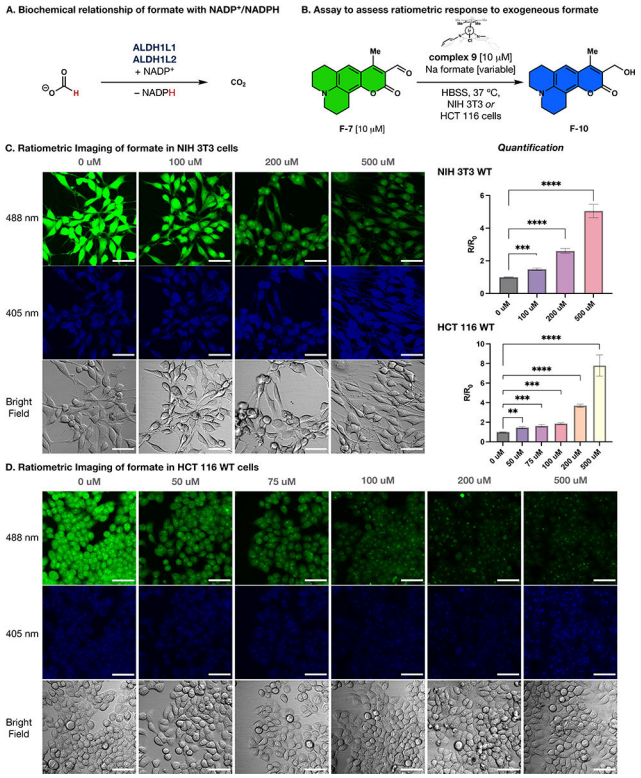

Figure 8.

(A) Formate is a one-carbon unit upstream of NADP+/NADPH cycling, where it is directly converted to NADPH by ALDH1L1/2 enzymes. (B) Two-component activity-based sensing (ABS) assay to detect formate using iridium-mediated transfer hydrogenation chemistry through a ratiometric fluorescence response *in vitro* and in live cells. (C) & (D) Representative confocal microscopy images of ratiometric fluorescence detection and imaging of formate fluxes in live NIH 3T3 WT (C) and HCT 116 WT (D) cells loaded with 10 μM **F-7** and complex **9**. Images were taken 60 min after the addition of vehicle (0 μM), 50 μM, 75 μM, 100 μM, 200 μM, and 500 μM sodium formate. Bright-field images of cells. Scale bar represents 10 μm in all images. R/R_0 denotes mean 405/488 excitation ratios of the cells treated with varying concentrations of sodium formate for 60 min relative to the mean 405/488 excitation ratios before formate addition; error bars denote SEM, n=4 biological replicates (2 technical replicates were averaged). ns > 0.05, *P ≤ 0.05, **P < 0.01, ***P < 0.001, ****P < 0.0001

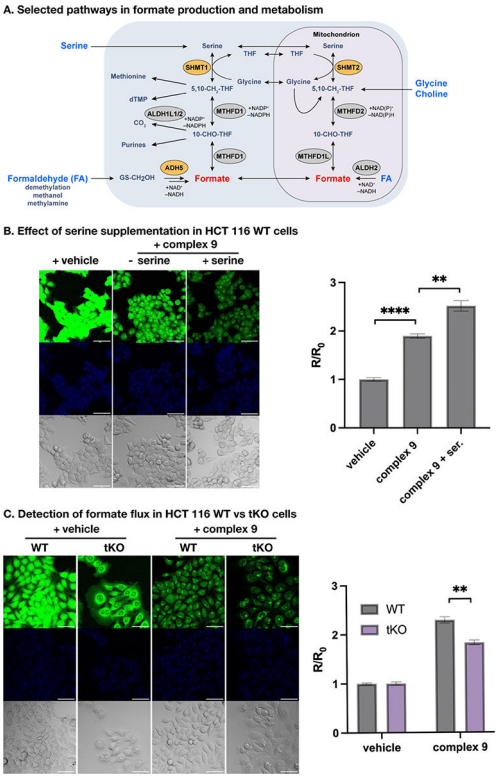

Figure 9.

Activity-based imaging of changes in formate fluxes in human colorectal carcinoma (HCT 116) cells with or without genetic alteration in biochemical pathways of one-carbon metabolism. (A) Selected biochemical pathways of formate production involved in one-carbon metabolism. (B) Serine supplementation (500 μM) in HCT 116 WT cells results in a significant ratiometric fluorescence increase with the two-component imaging system consisting of complex **9** (10 μM) and fluorophore **F-7** (10 μM), showing that formate production is sensitive to status of this amino acid nutrient. (C) Confocal microscopy images showing that HCT 116 cells with a *SHMT1/SHMT2/ADH5* triple knockout (tKO) produce a lower ratiometric response to the complex **9** (10 μM) and fluorophore **F-7** (10 μM) relative to the wild-type HCT 116 WT cell line, indicating that blocking serine and formaldehyde sources of formate leads to lower basal levels of this one-carbon unit in cells. R/R_0 denotes mean 405/488 excitation ratios of the HCT 116 (WT vs tKO) cells treated with varying concentrations of sodium formate for 60 min relative to the mean 405/488 excitation ratios of vehicle-treated cells; error bars denote SEM, n=4 biological replicates (2 technical replicates were averaged). ns > 0.05, *P ≤ 0.05, **P < 0.01, ***P < 0.001, ****P < 0.0001.